RSC Advances

PAPER

View Article Online
View Journal | View Issue

Cite this: *RSC Adv.*, 2021, **11**, 14017

The enhancement of ozone–liquid mass transfer performance in a PTFE hollow fiber membrane contactor using ultrasound as a catalyzer†

Bing Wang, *[ab] Huan Zhang,[a] Qingjie Meng,[c] Hongyang Ren,[a] Mingyang Xiong[a] and Chunyang Gao[a]

A comprehensive assessment of a polytetrafluoroethylene (PTFE) hollow fiber membrane contactor and ultrasound for intensifying ozone–liquid mass transfer was conducted simultaneously. The initial part of the study concentrates on the systematic analysis of the previous literature related to the reinforcement on the ozone–liquid mass transfer. In this paper, the introduction of a membrane contactor and ultrasound as a catalyzer that increased the mass transfer coefficient (K_La) may be partially attributed to the increase of the net surface area and the decrease of the mass transfer resistance, thus leading to the enhancement of the ozone mass transfer rate and acceleration of the ozone decomposition in solution. Results revealed that the maximum value of the K_La value was 0.7858 min^{-1} in the PTFE hollow fiber membrane contactor in the presence of the ultrasound, while only 0.5154 min^{-1} in a single ozone aeration at an intake flow of 300 L h^{-1}, ozone dosage of 32.38 mg L^{-1} and operating temperature of 293.15 K. A 52.46% improvement of the K_La value was obtained in the presence of the ultrasound. In addition, the dosage of sodium chloride appeared to have a positive correlation with K_La, but a negative correlation with the concentration of dissolved ozone. The sulfolane destruction by ozonation, ultrasound and the combination between the ozonation and ultrasound were performed to further verify the enhancement of the ozone mass transfer performance. It has been established that the O_3/US combined process was a promising method, giving the maximum degradation of sulfolane (96.5%) with the synergistic index as 2.41.

Received 19th January 2021
Accepted 2nd March 2021

DOI: 10.1039/d1ra00452b

rsc.li/rsc-advances

1. Introduction

It is well known that ozone has the characteristics of strong oxidation performance, environment protection and high effectiveness; it has also been widely observed and investigated for the wastewater treatment and ozone-based processes to improve the quality of water.[1–3] The total reaction rate of the ozonation process can be affected by both the reaction kinetics and mass transfer coefficient (K_La).[4] However, the main disadvantage of ozone is its low solubility and instability in aqueous solution, which limits the extent of its application. Ozonation processes are conventionally carried out by the gas bubble formation using ozone–water contactors, including porous diffusers, injector nozzles, bubble columns and venturi injectors.[5–8] However, in those cases, ozone–liquid transport is a rate-limiting process due to the size and distribution of ozone bubbles.[9] An alternative approach is to increase the ozone mass transfer from the gas phase to the liquid phase using membrane contactors.

Membrane contactors act as a convenient barrier between the gas and water phases, and offer several advantages of higher gas–water contact area, higher efficiency of ozone dissolution, no foaming and low-energy demand. Because of their non-polar structure, polymeric membranes employed for gas–liquid membrane contacting offer the advantage of hydrophobicity to differing degrees. Hollow fiber configurations can be produced with small diameters of a few μm, thus achieving a very high specific internal membrane surface area. Porous membranes with ozone durability are used as ozone–water membrane contactors, such as polytetrafluoroethylene (PTFE), polyvinylidene-fluoride (PVDF), polyethylene (PE) and polyvinylfluoride (PVF). The ozone durability of the above membrane contactors obeys the order of PTFE > PVDF > PE > PVF.[10] The commonly used porous membrane materials are PVDF and PTFE, both fluoropolymers, which show the strongest chemical stability among the polymer group, as the electronegativity of fluorine atoms and the absence of carbon double bonds in the structure prevent an ozone or OH-radical attack.[11] However, previous

[a]School of Chemistry and Chemical Engineering, Southwest Petroleum University, Chengdu 610500, P. R. China. E-mail: wangb@swpu.edu.cn; Fax: +86 24 83037306; Tel: +86 28 83037300

[b]Sichuan Provincial Key Laboratory of Environmental Pollution Prevention on Oil and Gas Fields and Environmental Safety, Chengdu 610500, P. R. China

[c]Hade Oil and Gas Development Department, PetroChina Tarim Oilfield Company, Korla 841000, P. R. China

† Electronic supplementary information (ESI) available. See DOI: 10.1039/d1ra00452b

studies indicate that PVDF is susceptible for material alterations, which may take place over time. Bamperng *et al.*[10] treated dye solutions with ozone membrane contactors, and observed an ozone flux decline of 30% for PVDF membranes compared to PTFE over 16 h. For the PTFE membranes, no property changes over time have been reported. In addition, PTFE is characterized as the high melting point, low solubility, high thermal stability, low friction, and low surface energy.[12,13] Thus, the PTFE hollow fiber membrane could be regarded as an ideal membrane contactor.

Another method of enhancing the mass transfer of ozone into solution is through the use of ultrasonic irradiation (US).[14–17] In the past few years, ultrasonic irradiation has a broad prospect of application in the catalysis aspect.[18–21] Ozone is decomposed thermolytically in the vapor phase of a cavitation bubble by sonolysis.[22] When ozone bubbles enter the ultrasound system, the turbulence would reduce the liquid film thickness.[23] Then, the K_La increases. In addition, one of the mechanical effects of ultrasound is the breakage of the ozone bubbles,[14] which leads to the larger specific surface area. Therefore, the ozone mass transfer coefficient K_La would increase in the presence of ultrasonic irradiation. Furthermore, hydroxyl radicals will be produced in the vapour phase of the cavitation bubbles during the ultrasonic process.[24]

As a clean and environmentally friendly energy source, the demand for natural gas is on the rise. For example, the development of China's natural gas industry has made significant progress in recent years, driven by the increasing domestic demand and the soaring oil and natural gas prices abroad.[25] Thus, the widespread use of sulfolane is all but inevitable. With the extensive application of sulfolane, it has been found in the overhaul wastewater. The most serious problems caused by large amounts of highly hazardous overhaul wastewater are generated by the sulfolane associated with the natural gas purification process, which lingers in the equipment, and then enters the effluent in the equipment maintenance period. Common symptoms of exposure to sulfolane are headache, nausea, tiredness, gastrointestinal upset, tremors, or convulsions. Furthermore, it can cause irritation of the eyes and skin allergies. Therefore, wastewater-containing sulfolane has become an environmental concern. Thus, it is of importance to explore efficient treatment processes for the removal of such pollutant.

The objectives of the present study were (a) to use ultrasound to improve the ozone–liquid mass transfer in the PTFE hollow fiber membrane contactor; (b) to analyze the enhancement mechanism of ozone mass transfer using ultrasound; (c) to evaluate the effect of operation parameters on the K_La value and dissolved ozone concentration, and (d) to investigate the synergistic effect between ultrasound and ozonation for removing sulfolane.

2. Overview of work done on the intensification of ozone–liquid mass transfer in recent years

Ozonation, as one of the effective advanced oxidation processes (AOPs), has been extensively used to remove refractory organics in wastewater. It is necessary to improve ozone–liquid mass transfer due to the relatively low solubility of ozone. Many interesting methods by vast scholars proposed for the enhancement of ozone–liquid mass transfer have been demonstrated in the recent past, and some of the recent investigations have been highlighted here to present a degree of confidence.

Graça *et al.*[26] investigated the ozone–water mass transfer enhancement in continuous mode using a macroscale oscillatory flow reactor provided with smooth periodic constrictions (OFR-SPC). The obtained results indicated that K_La increased with an increase in f (up to 4 Hz), x_0 (up to 15 mm), and the gas flow rate (up to 150 N cm^3 min^{-1}). Sabelfeld and Geißen[27] have studied the ozone mass transfer in a helically wounded hollow fiber membrane contactor, which is dependent on the operating conditions. In comparison, the high-ozone-dosage low-liquid velocities were favorable. Additionally, the mass transfer enhancement was related to the gas flow orthogonal to the helical wounded fibers at the fiber shell. The obtained results indicated that the helical structure of the hollow fibers of the ozone–liquid membrane contactor contributed to the high ozone flow rates and high ozone dissolved concentration, increasing the mass transfer coefficient. Ratnawati *et al.*[28] studied the effect of the ozone-containing gas flow rate (over a range of 2–5 L min^{-1}) and pH (over a range of 4–10) on the ozone mass transfer coefficient in a bubble column reactor. The obtained results indicated that a maximum K_La of 2.1×10^{-3} s^{-1} at pH 4 with a gas flow rate of 4 L min^{-1} was obtained. Stylianou *et al.*[29] investigated the ozone transfer to water using a tubular hydrophobized a-Al_2O_3 membrane contactor. The pH and ozone concentration values played a significant role in the dissolved ozone concentration, while the temperature has relatively little effect on the measured ozone. Abdullah *et al.*[30] studied the ozone–liquid mass transfer under semi-batch conditions in a bubble column, a baffled column and an oscillatory baffled reactor (OBR). The obtained results indicated that the ozone mass transfer efficiency increased from 57% using the baffled reactor to 92% with OBR when the liquid and gas superficial velocities were 0.3 and 3.4 cm s^{-1}, respectively. Ren *et al.*[4] investigated the effect of different superficial gas and liquid velocities on the overall liquid side volumetric mass transfer coefficient ($k_L\alpha$) in a novel microchannel reactor. As is well known, the reaction behavior of the multiphase reaction depends on the ozone mass transfer and the residence time in the microchannel. Kukuzaki *et al.*[31] investigated the ozone transfer with tubular hydrophilic and hydrophobized Shirasu porous glass (SPG) membranes based on the ozone absorption into water. It has been reported that the fluorocarbon functional group of an organosilane compound modified the surface of the SPG membranes. A maximum overall mass transfer coefficient (K_L) of 1.2×10^{-5} m s^{-1} was obtained for the 0.51 μm hydrophobized membrane. It can be observed that the K_L value for the hydrophobized SPG membranes was much larger, as compared to that obtained for the hydrophilic membrane (2.1×10^{-6} m s^{-1}). An enhanced turbulence at the surface of the membrane could contribute to the higher K_L values. Gao *et al.*[8] investigated the characteristics of the Karman contactor as an

ozonation unit by measuring the volumetric mass transfer coefficient of ozone (K_La), gas hold-up (ε_G), and bubble size. It has been observed that increasing the gas and liquid flow rates significantly enhances the rates of ozone absorption, owing to the small bubbles produced by the Karman contactor. The augmentation of small bubbles has increased the interfacial area of the gas–liquid contact, leading to the increase of K_La. Although the Karman contactor was expensive compared with other conventional bubble columns, its performance was satisfactory due to the high performance. Intensification of the ozone mass transfer using a reactor has been reported by Mitani *et al.*[32] This reactor was composed of a microporous stainless steel tubular gas diffuser, leading to a decrease in the gas bubble size and improvement in the overall mass transfer area. It was observed that as the liquid flow rate increased from 3.33 $\times$ 10^{-6} to 2.08 $\times$ 10^{-5} m^3 s^{-1}, the K_La value increased from 0.0223 to 0.316 s^{-1} in our system. In most studies, the gas flow rate had a positive influence on the ozone mass transfer coefficient. In contrast, the liquid flow rate was dominant in the rate of ozone mass transfer in this study. Farines *et al.*[33] investigated the influence of the superficial gas and liquid velocities on the ozone mass transfer using a co-current upflow reactor filled with granular silica gel. It was found that the dissolved ozone concentration depends on the technological parameters and conditions of the reactor. At steady state, increasing the gas velocity yields the increase in both overall mass transfer coefficient and dissolved ozone concentration. Hsu *et al.*[34] studied the ozone mass transfer from gaseous to solution using a new gas-inducing reactor. The effect of several operational parameters, namely agitation speed, superficial gas velocity, temperature and working liquid level on the ozone volumetric mass-transfer coefficient ($K_{L,O_3}a$), was investigated in a semi-batch system. The obtained experimental results indicated that an increase of the ozone volumetric mass-transfer coefficient could be attributed to the increase of the agitation speed, temperature, and superficial gas velocity. Jakubowski *et al.*[35] studied the ozone mass transfer using a confined plunging liquid jet contactor (CPLJC). The overall volumetric mass transfer coefficient (K_La) plays an important in the ozone mass transfer performance of the CPLJC. It was observed that increasing the volumetric gas flow rate (Q_G) leads to an increase of the interfacial area (a), thus K_La. It has been reported that the K_La value was in the 0.301–0.474 (s^{-1}) range.

Intensification of the ozone mass transfer using acoustic and hydrodynamic cavitations has been reported by Karamah *et al.*[36] The effect of the application of acoustic cavitations, hydrodynamic cavitations, and the combination of acoustic and hydrodynamic cavitations on the ozone mass transfer was observed using four process schemes. The obtained results presented a synergistic effect between the hydrodynamic and acoustic cavitations to improve the ozone mass transfer. The enhancement of the acoustic cavitation was higher than that of the hydrodynamic cavitation. The enhancement effect by the ozone mass transfer decreased in the order of combination of the hydrodynamic cavitation, sonication and ozonation > combination of sonication and ozonation > combination of hydrodynamic cavitation and ozonation. For the combination of both types of cavitation and ozonation, the enhancement of the chemical effect of cavitation was 3.68 times the mechanical effects. Weavers and Hoffmann[37] studied the sonolytic degradation of ozone using both closed and open continuous-flow systems in order to explore the influence of the mass transfer on the chemical reactivity under ultrasound. By measuring the mass transfer coefficient (K_La_2), it was observed that the O_3 mass transfer diffusing into the aqueous phase was increased. This can be explained in that the application of the ultrasonic waves improved the ozone–liquid mass transfer as a result of the sonolytic degradation of O_3, producing a larger driving force to accelerate the dissolution of gaseous O_3.

3. Experimental

3.1 Materials

The membrane contactors used in the present study were purchased from DD Water Group Co. (Zhejiang Province, China). Characterizations of the PTFE hollow fiber membrane contactors are as follows in Table 1 and Fig. S1.† The diameter distributions of the microbubbles were measured using the method described in the previous research.[38] All chemicals used in this study were of analytical grade. Deionized water freshly prepared in the laboratory was used in all experiments.

3.2 Experiment set-up

The experimental apparatus is constitutive of the membrane contactors and ultrasonic generation system, as shown in Fig. 1, which is made entirely of plexiglass (acrylic) with a breadth of 0.06 m, a depth of 0.06 m, and a height of 0.6 m. There were 20 membrane contactors, which were installed at the bottom of the reactor, and each PTFE hollow fiber membrane contactor was 150 mm in length. One end of the membrane contactor was positioned at the bottom of the reactor, and the other end was well sealed to ensure that ozone was introduced into the liquid phase through the membrane contactors.

Ozone was produced from extra-dry and high-purity oxygen by using a CF-G-3-20 g generator (Qingdao Guolin, China). The flow rate of ozone was controlled by a rotameter incorporated into the ozone generator. Varying the electricity of the ozone generator regulated the gaseous ozone concentration, as could be seen in Table S1.† The ultrasonic probe connected with an ultrasonic generator (MS-ZDB, 20 kHz, Handan City Meishun Machinery Co., Ltd) was arranged at the top of the reactor.

Table 1 Major physical properties of the PTFE hollow fiber membrane contactors

Membrane contactor parameters	Value
Mean pore diameter [μm]	0.22
Porosity [%]	83.8
External diameter [mm]	2.291
Wall thickness [mm]	0.453
Contact angle [°]	102.66

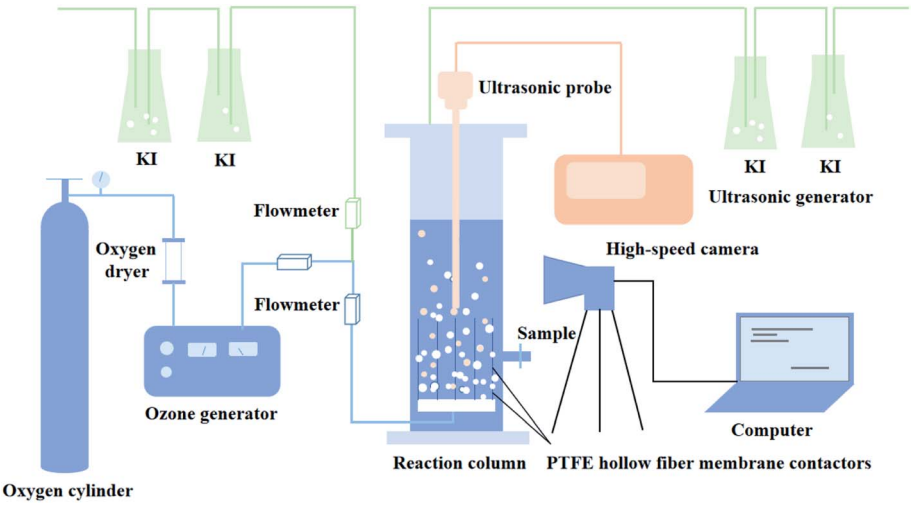

Fig. 1 Schematic diagram of the experimental apparatus.

Dissolved ozone concentrations were measured by indigo method.[39] The off-gas ozone leaving the reactor was trapped in gas absorption bottles containing 2% (w/v) KI solution. The pH value of the solution was buffered close to 3 by adding sulfuric acid solution, which depressed the ozone self-decomposition. The pH was determined using a pHS-3C meter.

One mL samples were taken at each interval, and were extracted with 1 mL dichloromethane. The analysis of the samples in dichloromethane was performed using an Agilent 6890 GC equipped with auto-sampler and Flame Ionization Detector (FID). The samples were injected to the GC, and chromatographic separation was made on a fused silica capillary column (ZB 5MSI, Phenomenex). High purity helium was used as the carrier gas with a head pressure of 250 kPa. The temperature of the injection port was set as 165 °C, and the injection was set on splitless mode with 5.00 μL injection volume. The initial temperature was set to 90, and then ramped to 175 °C with 10 °C min^{-1} rate, where it kept constant for 3 min. The FID detector temperature set at 250 °C.

Before the experimental operation, the reactor was pre-ozonated for 5 min to satisfy any ozone demand in the reactor, and then it was washed several times with distilled water to exclude any possible side effects.

3.3 Determination of K_La

The transformation rate of ozone into hydroxyl radicals is strongly pH-dependent. In principle, for pH < 7, this variable has a slight influence on the ozone decomposition. Therefore, the natural ozone self-decomposition can be neglected in this study (pH 3).

The mass transfer coefficient (K_La) (min^{-1}) in the ozonation process can be expressed as follows:

$$\frac{dc}{dt} = K_La(C_s - C) - r \quad (1)$$

where C_s, C, and r are the ozone equilibrium concentration, dissolved ozone concentration and ozone self-decomposition rate, respectively.

In which $r = 0$, then eqn (1) can be further rewritten as:

$$\ln\left[\frac{C_s}{C_s - C}\right] = K_La \times t \quad (2)$$

The slope of $\ln[C_s/(C_s - C)]$ against t is the K_La value.

4. Results and discussion

4.1 Effect of the operating parameters on the bubble size distribution

4.1.1 Effect of the aeration patterns. The aeration pattern is an important factor of influencing the bubble diameter. In this section, the aperture of the PTFE hollow-fiber membrane aerator and bubble rock aerator were 0.22 and 1.55 μm, respectively. Fig. 2 presented the frequency distribution of the bubble diameter with different aeration patterns. The peaks of the bubble diameter distribution of the hollow-fiber membrane aerator were located in a smaller diameter range (40–49.9 μm)

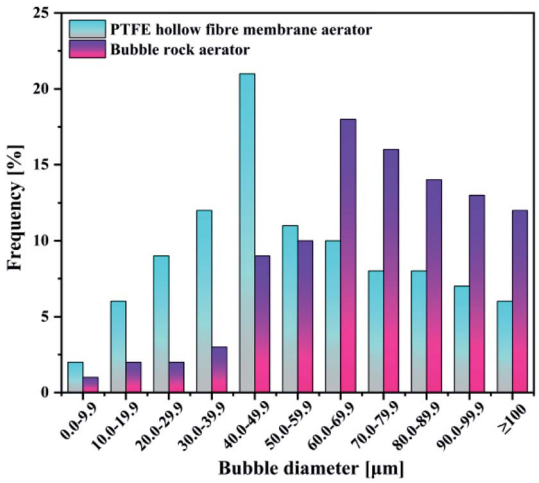

Fig. 2 Frequency distribution of the bubble size with different aeration patterns.

Table 2 Sauter mean radius under two different aeration patterns

Aeration patterns	PTFE hollow-fiber membrane	Bubble rock
Sauter mean radius [μm]	52.78	86.25

Table 3 Sauter mean radius under four different ultrasound powers

Ultrasound power [W]	0	1000	1500	2000
Sauter mean radius [μm]	52.78	35.62	32.81	30.49

than that of the bubble rock aerator (60–69.9 μm). Notably, the Sauter mean radius of the bubbles ranges from 52.78 μm to 86.25 μm with an increasing aperture from 0.22 μm to 1.55 μm, as illustrated in Table 2.

The balance between the fluid shear stress and surface tension force in solution caused the bubbles to form. Thus, the single spherical bubble diameter can be estimated by eqn (3).[40]

$$d_{eq} = \left(\frac{8 d_0 r}{C_D U_0^2 \rho_L}\right)^{0.5} \quad (3)$$

Here, d_0, r, C_D and U_0 are the orifice diameter, surface tension, drag coefficient and liquid velocity of the shear flow, respectively. As can be seen in eqn (3), the appreciable positive influence was observed between the bubble size and aperture of the aeration pattern. It agreed with the experimental results. According to the obtained results, the PTFE hollow-fiber membrane aerator was used in the subsequent studies.

4.1.2 Effect of the ultrasound power. In this work, a hollow-fiber membrane aerator was selected. The effect of the ultrasound power on the bubble size distribution is exhibited in Fig. 3.

Under the same total ultrasonic frequency (20 kHz) input condition, the percentage of small bubbles was found to increase (Fig. 3), while the Sauter mean radius of the bubbles decreased from 50.78 to 30.49 μm with the increasing power operated from 0 to 2000 W. The motion of the bubbles in this system was in the presence of ultrasound. The size of the bubbles was mainly determined by the bubble coalescence and breakup behavior, and ultrasonic action. For the same system, the motion of the bubbles kept a balance between the bubble coalescence and breakup in the absence of ultrasound.

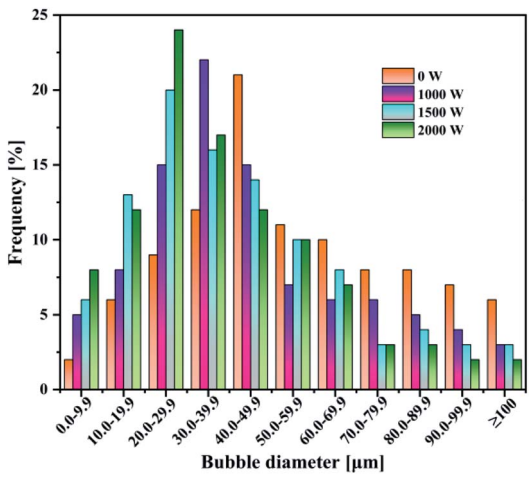

Fig. 3 Frequency distribution of the bubble size with different ultrasound powers.

However, a synthetic effect caused by such factors as cavitation effect, micro-jetting and turbulence has an obvious effect on the production of bubbles in the presence of ultrasound. These comprehensive effects destroyed the balance between the motion, growth, coalescence and breakup of the original bubbles, and caused much more violent turbulence in the gas–liquid two-phase flow to make more bubbles break up. Remarkably, the introduction of ultrasound decreased the mean radius of the bubbles (Table 3).

4.2 Effects of operating parameters on the ozone mass transfer

4.2.1 Effect of the aeration patterns. In this part, the experiments were carried out as in Section 4.1.1. The aeration patterns made a remarkable impact on the dissolved ozone concentration and $K_L a$. The obtained results are illustrated in Fig. 4 and Table 4.

As evident in Fig. 4(a), the concentration of dissolved ozone in the PTFE hollow-fiber membrane aeration was significantly higher than that of bubble rock aeration. $K_L a$ followed the same trend as the concentration of dissolved ozone (Fig. 4(b)). From Section 4.1.1, it can be seen that the bubble size produced in the PTFE hollow-fiber membrane aeration (52.78 μm) was smaller than that of bubble rock aeration (86.25 μm). The smaller bubbles offer the higher interfacial area for the ozone–liquid contact, which favors the ozone mass transfer. It was found that the 0.7858 and 0.2601 min^{-1} of $K_L a$ were obtained by the PTFE hollow-fiber membrane aeration and bubble rock aeration, respectively. The PTFE hollow-fiber membrane aeration was over triple the $K_L a$ value of the bubble rock aeration. It could be concluded that the bubble size has a great influence on the ozone mass transfer.

4.2.2 Effect of the gaseous ozone concentration. The gaseous ozone concentration could directly affect the ozone–liquid mass transfer efficiency. In this section, the dissolved ozone concentration and $K_L a$ under different gaseous ozone concentrations were investigated, as shown in Fig. 5 and Table 5.

As can be seen in Fig. 5(a), the concentration of dissolved ozone increased with increasing gaseous ozone concentration. The results indicated that an increase in the gaseous ozone concentration is beneficial to the mass transfer of ozone to some extent. An increase in the gaseous ozone concentration is expected to correspond with an increase in the equilibrium ozone concentration in solution, which can be explained by Henry's law,[41]

$$C_s = \frac{[O_3]_g}{H} \quad (4)$$

Table 4 The concentration of dissolved ozone and K_La in different aeration patterns

Aeration patterns	Dissolved ozone concentration (mg L^{-1})	K_La (min^{-1})
PTFE hollow-fiber membrane aerator	7.6093	0.5154
PTFE hollow-fiber membrane aerator with US	11.1071	0.7858
Bubble rock aerator	1.0472	0.1586
Bubble rock aerator with US	2.2964	0.2601

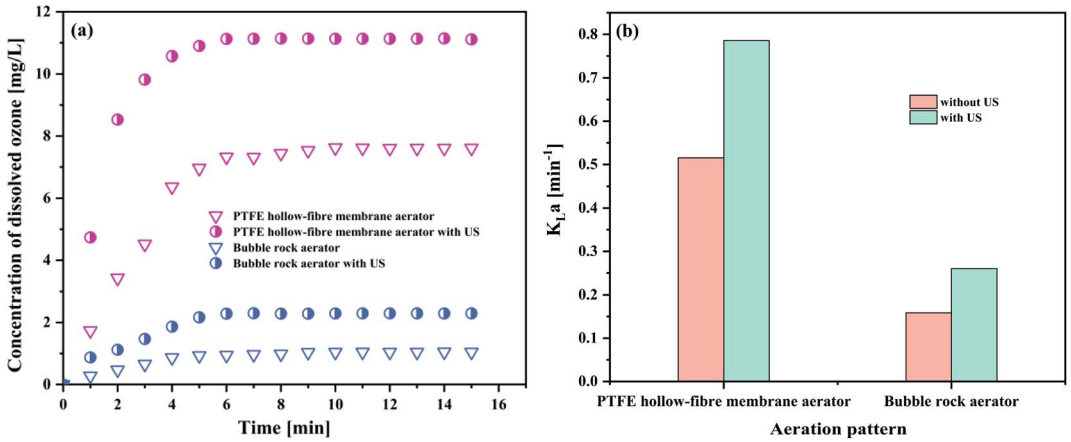

Fig. 4 Effect of the aeration patterns on (a) the concentration of dissolved ozone and (b) K_La (pH 3; intake flow rate 300 L h^{-1}; gaseous ozone concentration 32.38 mg L^{-1}; temperature 293.15 K; US power 1000 W).

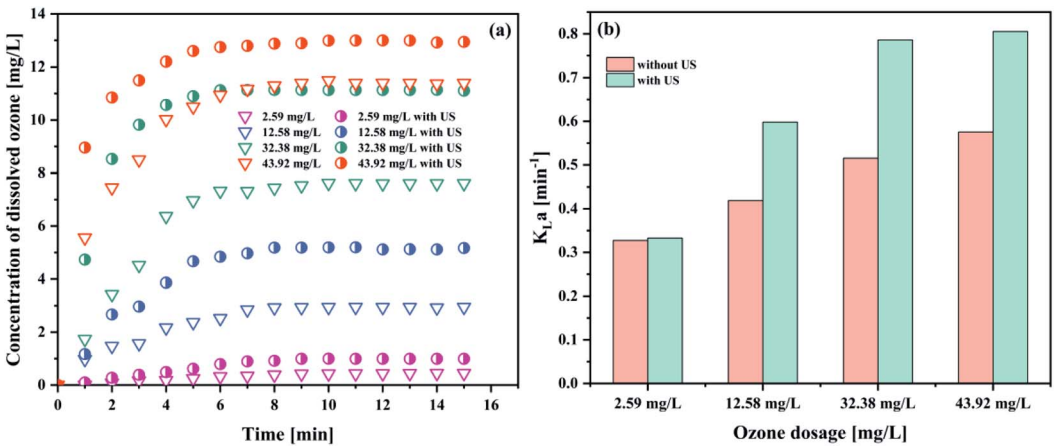

Fig. 5 Effect of gaseous ozone concentration on (a) the concentration of dissolved ozone and (b) K_La (pH 3; intake flow rate 300 L h^{-1}; temperature 293.15 K; US power 1000 W).

where H is the Henry law constant, and $[O_3]_g$ represents the ozone dosage.

An increase in the equilibrium ozone concentration could improve the ozone mass transfer driving force. The main driving force for ozone mass transfer is a concentration difference in the gas–liquid two-phase.[29,31] It has been reported that ozone in the solution would reach saturation at a fixed temperature. Influenced by the dissolution, reaction and decomposition of ozone, the ozone concentration in solution would stop continually increasing when it was saturated at a fixed ozone input as the reaction time was prolonged and obtained a balance in solution. The ozone mass transfer from gas to liquid is mainly controlled by liquid film. This leads to the increase of K_La (Fig. 5(b)). It was observed that the introduction of ultrasound increased the K_La value to 0.7858 min^{-1}, compared to 0.5154 min^{-1} of the ozonation in the absence of ultrasound in the PTFE hollow fiber membrane contactors, suggesting that the addition of ultrasound can contribute to the

Table 5 The concentration of dissolved ozone and K_La in different gaseous ozone concentrations

Gaseous ozone concentration	Dissolved ozone concentration (mg L^{-1})	K_La (min^{-1})
2.59 mg L^{-1}	0.4471	0.3273
2.59 mg L^{-1} with US	0.9930	0.3328
12.58 mg L^{-1}	2.9469	0.4187
12.58 mg L^{-1} with US	5.1689	0.5980
32.38 mg L^{-1}	7.6093	0.5154
32.38 mg L^{-1} with US	11.1071	0.7858
43.92 mg L^{-1}	11.3943	0.5755
43.92 mg L^{-1} with US	12.9430	0.8053

mass transfer of ozone dissolved into solution. Similar results have also been reported by Weavers *et al.*[37] for the enhancement of ozone mass transfer using ultrasound. The local turbulence created by ultrasonic cavitation helps to decrease the mass transfer resistance for the ozone–liquid transfer.[42] Considering the energy consumption and exhaust ozone, 32.38 mg L^{-1} was used for the following studies.

4.2.3 Effect of the intake flow rate. In this part, the effect of the ozone intake flow rate varying from 100 to 500 L h^{-1} on the ozone mass transfer was studied, and is presented in Fig. 6 and Table 6.

As can be seen in Fig. 6(a), the equilibrium ozone concentrations increased with an increase in the intake flow rate, ranging from 100 L h^{-1} to 300 L h^{-1} and 100 L h^{-1} to 200 L h^{-1} in both ozone system and the combination between ozone and ultrasound system, respectively. Similar results were reported in the literature.[38] In contrast, the K_La value increased first and then gradually decreased (see Fig. 6(b)). The maximum K_La value reached (0.7858 min^{-1}) was higher than that of the condition without ultrasound (0.5154 min^{-1}). A 52.5% improvement of the K_La value was obtained with the introduction of ultrasound, indicating that ultrasound could promote the mass transfer performance. Ultrasound appears to be a promising way to overcome the transfer limitations and improve the ozone mass transfer, compared to the same process without ultrasonication. It was observed that K_La increased due to the turbulence and surface renewal. Moreover, the rising velocity of the small ozone bubbles that produced the membrane contactors increased with the increasing intake flow rate. Thus, small bubbles were less likely to coalesce into larger bubbles. As is well known, the ozone mass transfer resistance was mainly controlled by the liquid phase. Increasing the intake flow rate caused a greater turbulence between the gas phase and the aqueous phase, which is conducive to the mixing of the gas–liquid two phases. It can be inferred that the faster ozone intake flow rate enhanced the mixing degree between the ozone–liquid two-phase, resulting in a decreased mass transfer resistance; thus, enhancing the ozone mass transfer coefficient. In contrast, the ozone intake flow rate was too fast to have enough time to collapse in the bulk solution, which caused the poor ozone mass transfer performance. Hence, based on the obtained results, the ozone intake flow rate of 300 L h^{-1} was used in the subsequent studies.

4.2.4 Effect of the operating temperature. The operating temperature has an impact on the solubility, decomposition rate, and stability of the ozone molecules in solution. In this

Table 6 The concentration of dissolved ozone and K_La on different intake flow rates

Intake flow rate	Dissolved ozone concentration (mg L^{-1})	K_La (min^{-1})
100 L h^{-1}	3.1798	0.2602
100 L h^{-1} with US	11.9565	0.3738
200 L h^{-1}	4.2491	0.3332
200 L h^{-1} with US	12.9491	0.4825
300 L h^{-1}	7.6093	0.5154
300 L h^{-1} with US	11.1071	0.7858
400 L h^{-1}	6.6267	0.4343
400 L h^{-1} with US	10.1673	0.5381
500 L h^{-1}	5.7404	0.3604
500 L h^{-1} with US	7.0174	0.4900

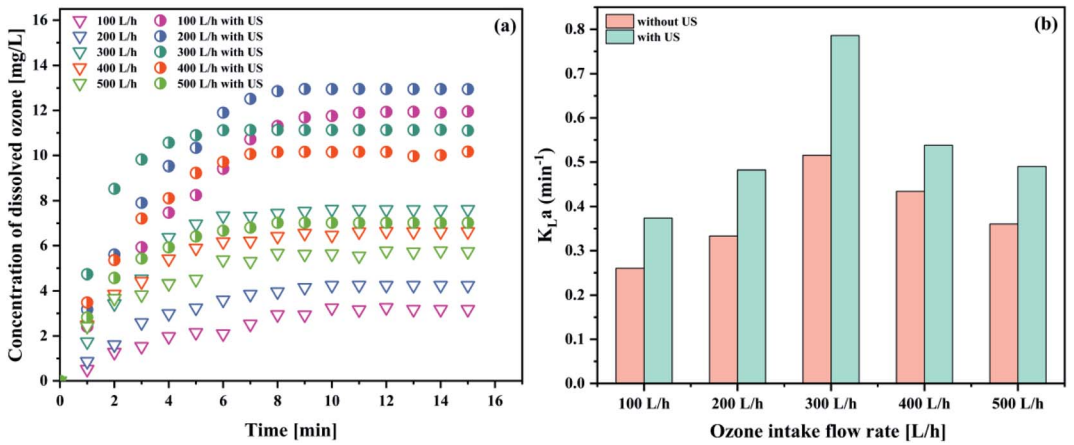

Fig. 6 Effect of the intake flow rate on (a) the concentration of dissolved ozone and (b) K_La (pH 3; gaseous ozone concentration 32.38 mg L^{-1}; temperature 293.15 K; US power 1000 W).

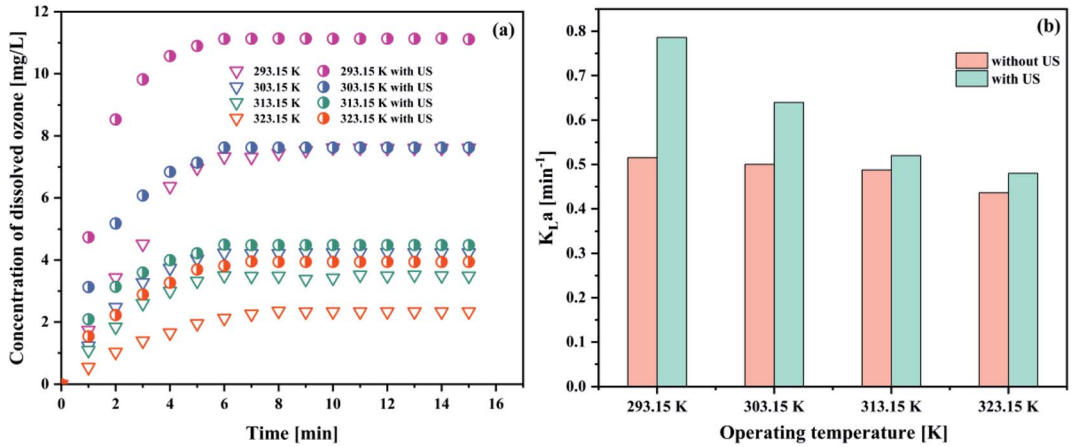

Fig. 7 Effect of operating temperature on (a) the concentration of dissolved ozone and (b) K_La (pH 3; intake flow rate 300 L h^{-1}; gaseous ozone concentration 32.38 mg L^{-1}; US power 1000 W).

Table 7 The concentration of dissolved ozone and K_La in different operating temperatures

Operating temperature	Dissolved ozone concentration (mg L^{-1})	K_La (min^{-1})
293.15 K	7.6093	0.5154
293.15 K with US	11.1071	0.7858
303.15 K	4.2419	0.5002
303.15 K with US	7.6242	0.6402
313.15 K	3.4887	0.4875
313.15 K with US	3.4845	0.5211
323.15 K	2.3343	0.4364
323.15 K with US	3.9435	0.4801

section, the effects of various temperatures from 293.15 to 323.15 K on the dissolved ozone concentration and K_La were investigated, and are presented in Fig. 7 and Table 7.

The results in Fig. 7(a and b) showed that the ozone equilibrium concentration and K_La in water decreased with the increase of the operating temperature in each system, indicating the increase of temperature against ozone mass transfer. Both ozone equilibrium concentration and K_La value could be boosted by the addition of ultrasound. The higher the temperature, the lower the ozone equilibrium concentration in solution. This phenomenon can be explained by Henry's constants (273–333 K):[43]

$$\log\left(\frac{H}{\text{kPa m}^3\ \text{mol}^{-1}}\right) = 5.12 - \frac{1230}{T(\text{K})} \quad (5)$$

The similar trends of the results were also reported in the literature.[44–46] When the operation temperature increased from 293.15 to 323.15 K with the decrease of the dissolved ozone concentration, this caused the decrease of the ozone mass transfer driving force, and hence decreased K_La. It was found that with an increase in the temperature, the viscosity and/or surface tension decreased, resulting in a reduction of the cavitation intensity. Thus, the liquid phase resistance increased. Considering the obtained results and associated discussion, 293.15 K was established as the optimum operating temperature for further studies.

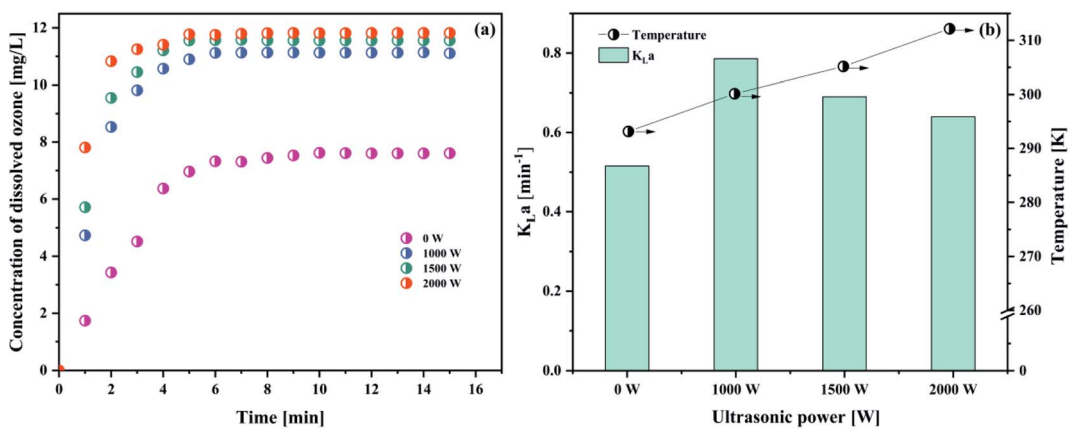

Fig. 8 (a) Variations in the dissolved ozone concentration with time under different ultrasonic powers, and (b) the corresponding K_La value and system temperature (pH 3; intake flow rate 300 L h^{-1}; gaseous ozone concentration 32.38 mg L^{-1}; temperature 293.15 K).

Table 8 The concentration of dissolved ozone and K_La in different ultrasonic powers

Ultrasonic powers	Dissolved ozone concentration (mg L^{-1})	K_La (min^{-1})
0 W	7.6093	0.5154
1000 W	11.1071	0.7858
1500 W	11.5598	0.6902
2000 W	11.8260	0.6401

4.2.5 Effect of the ultrasonic power. Ultrasound power has great significance for acoustic cavitation. This is because it has an effect on the collapse intensity, number of cavitation bubbles and economy of the cavitation system.[47] To our knowledge, the ultrasound contributes to the improvement of the ozone transfer performance.[48]

As observed in Fig. 8(a) and Table 8, it was demonstrated that increasing the ultrasonic power (from 1000 to 2000 W) has a positive effect on the dissolved ozone concentration. However, when the ultrasound power increases (from 1000 to 2000 W), the K_La value will decrease (from 0.7858 min^{-1} to 0.6400 min^{-1}) (Fig. 8(b)). In the same condition, a blank test (ultrasonic power is 0) was also carried out.

The result was attributed to the following reasons. On the one hand, ultrasound could create the mechanical effects, including a greater mixing and break up of the ozone bubble,[14,37] which increased the specific surface area (seen Section 4.1.2). Tsochatzidis *et al.*[49] reported that the increase of the input ultrasonic power at a constant ultrasound frequency increases the opportunity of the cavitation bubble collapse. The acoustic streaming accelerated the interfacial turbulence by cavitation bubbles collapse at the interface of the gas–liquid phase. Thus, the K_La value increased in the presence of ultrasound. On the contrary, when the ultrasound power reached a certain value, cavitation would tend to saturation. When the ultrasound power further increased, the cavitation bubbles would be too big to collapse, and an acoustic screen forms in this system. As a result, this led to a decrease in the K_La value. In addition, with higher ultrasound power, the temperature in solution would increase. As is well known, the higher temperature is very unfavourable for the solubility of ozone in water. Considering the obtained results and lower energy waste, the optimum ultrasonic power was 1000 W.

4.2.6 Presence of sodium chloride. Sodium chloride has been used for the improvement of the chemical reactions in the presence of ultrasound.[50] It was also reported that the addition of sodium chloride gave higher gas phase holdup and mass-transfer coefficient due to the noncoalescing action of the electrolyte.[14,29] Therefore, it is necessary to investigate the dissolved ozone concentration and K_La value trends in the existence of sodium chloride.

As could be seen from Fig. 9 and Table 9, the introduction of sodium chloride was negatively correlated with the concentration of dissolved ozone, and positively correlated with the K_La value. The highest K_La value was obtained with the dosage of NaCl of 1500 mg L^{-1} (1.1144 min^{-1}). To the best of our knowledge, the addition of NaCl could decrease the gas solubility.[51] However, the bubble diameter decreased with an increase in the salt concentration.[52] Similar results were also reported by Walker *et al.*[53] The increase of K_La attributed to the

Table 9 The concentration of dissolved ozone and K_La in different NaCl concentrations

NaCl concentrations	Dissolved ozone concentration (mg L^{-1})	K_La (min^{-1})
0 mg L^{-1}	7.6093	0.5154
0 mg L^{-1} with US	11.1071	0.7858
500 mg L^{-1}	5.2646	0.6065
500 mg L^{-1} with US	9.1563	0.8457
1500 mg L^{-1}	3.2598	0.7831
1500 mg L^{-1} with US	7.5644	0.9158
2000 mg L^{-1}	2.2661	0.8632
2000 mg L^{-1} with US	4.6545	1.1144

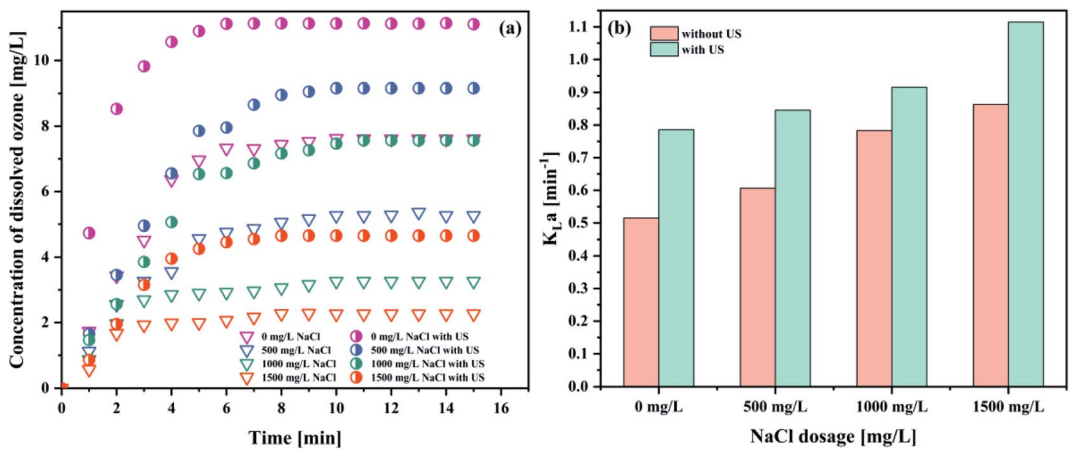

Fig. 9 Effect of NaCl on (a) the concentration of dissolved ozone and (b) K_La (pH 3; intake flow rate 300 L h^{-1}; gaseous ozone concentration 32.38 mg L^{-1}; US power 1000 W; temperature 293.15 K).

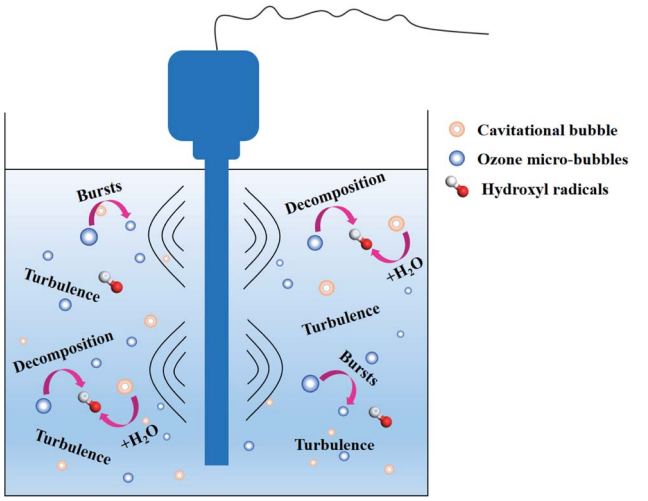

Fig. 10 Proposed enhancement pathway for ozone mass transfer by ultrasound.

larger available gas–liquid interfacial area. On the one hand, the ionization of NaCl makes the production of vast quantities of charged ions in solution. The electrical adsorption of these ions enhanced the liquid film of the bubble. So, the coalescence of the bubbles was suppressed, causing the decrease of the bubble size.[52] On the other hand, the presence of NaCl lowers the zeta potential of the bubble interface in water, thereby increasing the bubble stability in the system, leading to the decrease of the bubble size.[54] In addition, the surface tension in the water increased with the increase in the concentration of NaCl solution. Furthermore, the bubble size decreases with increasing surface tension.[55] These small bubbles in the system subsequently increase the net gas–liquid interfacial area. At the same time, a decrease in the bubble diameter prolongs the bubble residence time in liquids.[52] This would increase the ozone mass transfer from the gas phase to the liquid phase.[51] From the data obtained, it seems that the degree of increase in the mass transfer coefficient with an increase of the interfacial area is greater than the decrease caused by the decrease in ozone solubility due to the addition of NaCl. The K_La value increased with the NaCl concentration. Nevertheless, this is in disagreement with the results of other researchers, who showed that the changes in the surface tension exerted considerable influence on the bubble size, but it had no significant impact on the mass transfer.[56] In short, the order-of-magnitude increase in the interfacial area at high salt concentration is the chief cause of the high K_La value.[52] Therefore, the K_La value increases.

4.3 Discussion on the enhancement mechanism

According to the comprehensive results obtained, the enhancement of the ozone mass transfer in aqueous medium increased with the introduction of ultrasound into the ozone system (Fig. 10). Ultrasonic cavitation bubbles were subjected to the surface tension, viscous force, inertia force and buoyancy in the fluid, and collapsed when the gas–liquid phase interface was precipitated. The periodic precipitation of these bubbles from the phase interface caused the local fluids near the gas–liquid interface to be periodically replaced, leading to the strong disturbance on the liquid surface and resulting in the deformation and turbulence of the phase interface, thus renewing the fluids on the interface surface. This is an important hydrodynamic instability phenomenon. The interfacial turbulence causes mass transfer in the form of convection, greatly reducing the mass transfer resistance. In addition, the contact area of ozone with water will be increased due to the ultrasound with the breakage of ozone bubbles, which can significantly enhance the whole dissolution process. Many ozone bubbles and cavitation bubbles previously existing in the solution became larger. When the size of the bubbles exceeded a certain value, the cavitation bubble and ozone bubbles encountered catastrophic collapse. The bubble radii become increasingly small. In addition, the cavitation bubbles gradually release energy through implosions to attack the ozone bubbles, making them easily decompose in the liquid. According to the note

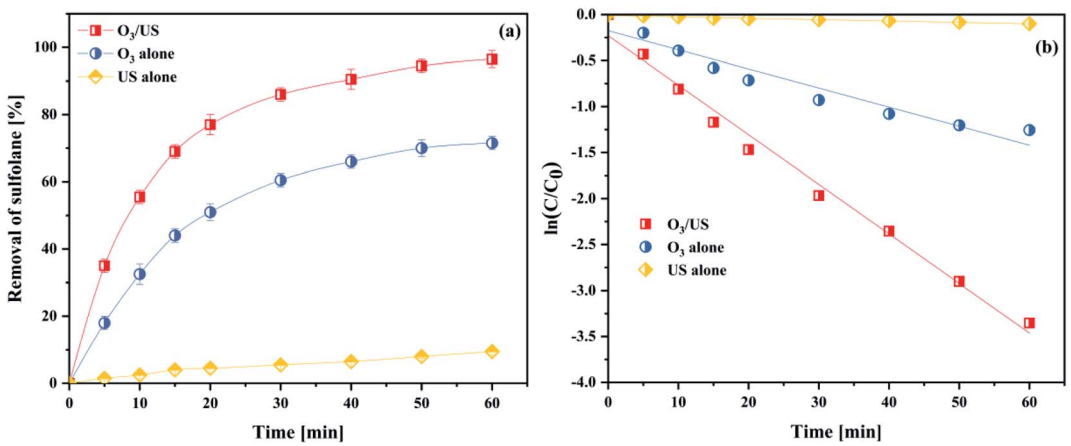

Fig. 11 (a) Comparison of different reaction systems in terms of the destruction of sulfolane; (b) kinetic data fitting for the sulfolane removal rate in different reaction systems (intake flow rate 300 L h^{-1}; gaseous ozone concentration 32.38 mg L^{-1}; US power 1000 W; temperature 293.15 K; initial sulfolane concentration 200 mg L^{-1}).

above, the ultrasound irradiation increased the mass transfer and decomposition of ozone.

4.4 Removal efficiency of sulfolane in different processes

To further investigate the synergy of ultrasonic and ozone, we take sulfolane as the model pollutant and use the removal rate of sulfolane to be the targets, conducting the applied research to the oxidation capability in ozonation, ultrasound (US) and ozonation/ultrasound systems, respectively. The results are shown in Fig. 11(a). As shown in Fig. 11(a), the degradation effect of sulfolane obeyed the order of O_3/US > O_3 > US. About 96.5% of sulfolane was removed within 60 min, while only 9.5% of sulfolane was removed by US alone. From the kinetic analysis, it has been established that the sulfolane removal rate followed pseudo-first-order kinetics with trends being displayed in Fig. 11(b), and the obtained values of the kinetic rate constants are given in Table S2.†

The introduction of ultrasound to ozonation further enhanced the sulfolane degradation, indicating that ultrasound increased the ozone mass transfer and accelerated the production of $OH^{\bullet}$ in the ozonation process. The synergistic index (E) for the combined process of O_3/US was calculated as follows:

$$E = \frac{k_{O_3/US}}{k_{US} + k_{O_3}} \quad (6)$$

Considering the results of Table S2,† we obtained the rate constants for the combined process of ozonation, and found that it was 2.41 times higher than that of adding them independently for sonication and ozonation. This phenomenon illuminated a good synergistic effect between ultrasound and ozonation. With larger values of E, in particular, better synergistic effects were achieved.

5. Conclusions

The finding of the present study proved that ultrasound was a more favorable choice for the enhancement of ozone mass transfer than separate experiments involving only ultrasonic irradiation alone or single ozonation. The increase of ozone mass transfer in the presence of ultrasound may be partially attributed to (1) a reduction of the mass transfer resistance; (2) a larger contact area between ozone and liquid solution; (3) renewal of the fluids on the interface surface. It was obvious that the presence of ultrasound heightens K_La to 0.7858 min^{-1} compared to 0.5151 min^{-1} of the ozone system. The increase of K_La was derived from the increase of the ozone mass transfer and the acceleration of the ozone decomposition. The presence of NaCl in the liquid decreases the bubble size. It was also shown that the K_La value increases, and the concentration of dissolved ozone decreases with a higher concentration of NaCl. The destruction of sulfolane was further performed to investigate the enhancement of the ozone–liquid mass transfer in the PTFE hollow fiber membrane contactor in the presence of ultrasound. It was observed that the degradation efficiency of sulfolane by O_3–US and O_3/US follows the order of O_3/US > O_3 > US.

Author contributions

Project administration, Bing Wang; writing-original draft preparation, Huan Zhang; writing-review and editing, Qingjie Meng and Hongyang Ren; comments and suggestions, Bing Wang; data curation, Mingyang Xiong and Chunyang Gao.

Conflicts of interest

The authors declare no competing financial interests.

Acknowledgements

This work was carried out with the financial support of the "Double First-Class" University Project from Southwest Petroleum University (2019cxzd028), and the Technology Innovation R&D Project of Chengdu (2019-YF05-00066-SN).

References

1 M. S. Kim, D. Cha, K. M. Lee, H. J. Lee, T. Kim and C. Lee, *Water Res.*, 2020, **169**, 115230.
2 W. Fan, W. G. An, M. X. Huo, W. Yang, S. Y. Zhu and S. S. Lin, *Sep. Purif. Technol.*, 2020, **238**, 116484.
3 Y. Huang, M. Liang, L. Ma, Y. Wang, D. Zhang and L. Li, *Environ. Pollut.*, 2021, **268**, 115722.
4 J. Ren, S. He, C. Ye, G. Chen and C. Sun, *Chem. Eng. J.*, 2012, **210**, 374–384.
5 X. Li, F. Ma, Y. Li, H. Zhang, J. Min, X. Zhang and H. Yao, *Chem. Eng. J.*, 2020, **389**, 124411.
6 S. Pathapati Srikanth, L. Mazzei Angelo, R. Jackson James, K. Overbeck Paul and P. Bennett Justin, *Ozone: Sci. Eng.*, 2016, **38**, 245–252.
7 C. Shan, Y. Xu, M. Hua, M. Gu, Z. Yang, P. Wang, Z. Lu, W. Zhang and B. Pan, *Chem. Eng. J.*, 2018, **338**, 261–270.
8 M. T. Gao, M. Hirata and H. Takanashi, *Sep. Purif. Technol.*, 2005, **42**, 145–149.
9 A. A. Kulkarni, *Ind. Eng. Chem. Res.*, 2007, **46**, 2205–2211.
10 S. Bamperng, T. Suwannachart, S. Atchariyawut and R. Jiraratananon, *Sep. Purif. Technol.*, 2010, **72**, 186–193.
11 D. S. Pines, K. N. Min, S. J. Ergas and D. A. Reckhow, *Ozone: Sci. Eng.*, 2005, **27**, 209–217.
12 R. Shu, R. Shen and J. Liu, *Eng. Failure Anal.*, 2021, **122**, 105222.
13 Y. Sawae, T. Morita, K. Takeda, S. Onitsuka, J. Kaneuti, T. Yamaguchi and J. Sugimura, *Tribol. Int.*, 2021, 106884.
14 S. A. Hewage, J. H. Batagoda and J. N. Meegoda, *Environ. Eng. Sci.*, 2020, **38**, 521–534.
15 Q. Zhao, M. Li, K. Zhang, K. Wang, H. Wang, S. Meng and R. Mu, *J. Environ. Manage.*, 2020, **262**, 110356.
16 S. Chandak, P. K. Ghosh and P. R. Gogate, *Process Saf. Environ. Prot.*, 2020, **137**, 149–157.
17 V. V. Patil, P. R. Gogate, A. P. Bhat and P. K. Ghosh, *Sep. Purif. Technol.*, 2020, **239**, 116594.

18 Q. W. Gui, T. Fan, S. N. Ying, L. Yang, G. Tao, J. X. Tang, J. Y. Chen, C. Zhong and W. M. He, *Chin. Chem. Lett.*, 2020, **31**, 3241–3244.
19 W. Chao, L. H. Lu, A. Z. Peng, G. K. Jia, C. Peng, C. Zhong, Z. Tang, W. M. He and X. Xu, *Green Chem.*, 2018, **20**, 3683–3688.
20 N. H. Ince, G. Tezcanli, R. K. Belen and G. Apikyan, *Appl. Catal., B*, 2001, **29**, 167–176.
21 X. Xiong, B. Wang, W. Zhu, K. Tian and H. Zhang, *Catalysts*, 2018, **9**, 678–688.
22 A. Ziylan and N. H. Ince, *Catal. Today*, 2015, **240**, 2–8.
23 Y. Shen, Q. Xu, R. Wei, J. Ma and Y. Wang, *Ultrason. Sonochem.*, 2017, **38**, 681–692.
24 X. Y. Ma, Y. Q. Cheng, Y. J. Ge, H. D. Wu, Q. S. Li, N. Y. Gao and J. Deng, *Ultrason. Sonochem.*, 2018, **40**, 763–772.
25 Z. Y. Wang, D. K. Luo and L. L. Liu, *Energy Rep.*, 2018, **4**, 351–356.
26 C. A. L. Graça, R. B. Lima, M. F. R. Pereira, A. M. T. Silva and A. Ferreira, *Chem. Eng. J.*, 2020, **389**, 124412.
27 M. Sabelfeld and S. Geißen, *J. Membr. Sci.*, 2019, **574**, 222–234.
28 R. Ratnawati, A. K. Dyah, S. Purbo and P. Aji, *MATEC Web Conf.*, 2018, **156**, 2015.
29 S. K. Stylianou, M. Kostoglou and A. I. Zouboulis, *Ind. Eng. Chem. Res.*, 2016, **28**, 7587–7597.
30 A. Abdullah, C. Paul, H. Adam and Z. Kui, *Chem. Eng. Process.*, 2014, **84**, 82–89.
31 M. Kukuzaki, K. Fujimoto, S. Kai, K. Ohe, T. Oshima and Y. Baba, *Sep. Purif. Technol.*, 2010, **72**, 347–356.
32 M. M. Mitani, A. A. Keller, O. C. Sandall and R. G. Rinker, *J. Environ. Eng.*, 2005, **27**, 45–51.
33 V. Farines, S. Baig, J. Albet, J. Molinier and C. Legay, *Chem. Eng. J.*, 2003, **91**, 67–73.
34 Y. C. Hsu, T. Y. Chen, J. H. Chen and C. W. Lay, *Ind. Eng. Chem. Res.*, 2002, **41**, 120–127.
35 C. A. Jakubowski, B. W. Atkinson, P. Dennis and G. M. Evans, *Ozone: Sci. Eng.*, 2003, 1–12.
36 E. F. Karamah, B. Setijo and W. W. Purwanto, *Ozone: Sci. Eng.*, 2013, **35**, 482–488.
37 L. K. Weavers and M. R. Hoffmann, *Environ. Sci. Technol.*, 1998, **32**, 3941–3947.
38 B. Wang, X. Xiong, Y. Shui, Z. Huang and K. Tian, *Chem. Eng. J.*, 2019, **375**, 678–688.
39 H. Bader and J. Hoigné, *Water Res.*, 2013, **15**, 449–456.
40 S. E. Forresterc and C. D. Rielly, *Chem. Eng. Sci.*, 1998, **53**, 1517–1527.
41 Y. Wang, H. Zhang, L. Chen, S. Wang and D. Zhang, *Sep. Purif. Technol.*, 2012, **84**, 138–146.
42 P. R. Gogate, S. Mededovic-Thagard, D. Mcguire, G. Chapas, J. Blackmon and R. Cathey, *Ultrason. Sonochem.*, 2014, **21**, 590–598.
43 E. Rischbieter, H. Stein and A. Schumpe, *J. Chem. Eng. Data*, 2013, **45**, 338–340.
44 R. H. Huang, H. H. Yan, L. S. Li, D. Y. Deng, Y. H. Shu and Q. Y. Zhang, *Appl. Catal., B*, 2011, **106**, 264–271.
45 M. Mehrjouei, S. Müller and D. Möller, *Chem. Eng. J.*, 2015, **263**, 209–219.
46 J. Wang and Z. Bai, *Chem. Eng. J.*, 2017, **312**, 79–98.
47 S. Raut-Jadhav, D. V. Pinjari, D. R. Saini, S. H. Sonawane and A. B. Pandit, *Ultrason. Sonochem.*, 2016, **31**, 135–142.
48 M. Mischopoulou, P. Naidis, S. Kalamaras, T. A. Kotsopoulos and P. Samaras, *Renewable Energy*, 2016, **96**, 1078–1085.
49 N. A. Tsochatzidis, P. Guiraud, A. M. Wilhelm and H. Delmas, *Chem. Eng. Sci.*, 2001, **56**, 1831–1840.
50 J. D. Seymour and R. B. Gupta, *Ind. Eng. Chem. Res.*, 1997, **36**, 3453–3457.
51 K. Ajay, P. R. Gogate, A. B. Pandit, D. Henzi and W. A. Marie, *Ind. Eng. Chem. Res.*, 2004, **43**, 1812–1819.
52 A. Kawahara, M. Sadatomi, F. Matsuyama, H. Matsuura, M. Tominaga and M. Noguchi, *Exp. Therm. Fluid Sci.*, 2009, **33**, 883–894.
53 A. B. Walker, C. Tsouris, D. W. Depaoli and K. Thomas Klasson, *Ozone: Sci. Eng.*, 2001, **23**, 77–87.
54 M. Takahashi, *J. Phys. Chem. B*, 2005, **109**, 21858–21864.
55 M. Ramezani, M. J. Legg, A. Haghighat, Z. Li, R. D. Vigil and M. G. Olsen, *Chem. Eng. J.*, 2017, **319**, 288–296.
56 P. Kováts, D. Thévenin and K. Zhringer, *Int. J. Multiphase Flow*, 2019, **123**, 103174.